Effect of the Length and Effective Diameter of F-Actin on the Filament Orientation in Liquid Crystalline Sols Measured by X-Ray Fiber Diffraction

Toshiro Oda,* Kouji Makino,*# Ichiro Yamashita,* Keiichi Namba,* and Yuichiro Maéda*
*International Institute for Advanced Research, Matsushita Electric Industrial Co., Kyoto 619-0237, and #Department of Molecular Biology, Faculty of Science, Nagoya University, Nagoya 464-01, Japan

ABSTRACT We examined factors that affect the filament orientation in F-actin sols to prepare highly well-oriented liquid crystalline sols suitable for x-ray fiber diffraction structure analysis. Filamentous particles such as F-actin spontaneously align with one another when concentrated above a certain threshold concentration. This alignment is attributed to the excluded volume effect of the particles. In trying to improve the orientation of F-actin sols, we focused on the excluded volume to see how it affects the alignment. The achievable orientation was sensitive to the ionic strength of the solvent; the filaments were better oriented at lower ionic strengths, where the effective diameter of the filament is relatively large. Sols of longer filaments were better oriented than those of shorter filaments at the same concentration, but the best achievable orientation was limited, probably because of the filament flexibility. The best strategy for making well-oriented F-actin sols is therefore to concentrate F-actin filaments of relatively short length (<1 μm) by slow centrifugation in a low-ionic-strength solvent (<30 mM).

INTRODUCTION

Actin plays important roles in many biological events, such as cell division and cell motility. To understand the molecular mechanism in these events, it is crucial to know the atomic structure of F-actin as well as G-actin, for which multiple numbers of crystal structures have been solved (Kabsch et al., 1990; McLaughlin et al., 1993; Schutt et al., 1993). Many studies on the F-actin structure have also been reported, which include studies by electron microscopy (e.g., Hanson and Lowy, 1963; Milligan et al., 1990) and x-ray fiber diffraction (Popp et al., 1987; Holmes et al., 1990). The x-ray fiber diffraction method, using well-oriented filament sols, is a potentially powerful tool for atomic resolution structural analysis of fibrous assembly of macromolecules with helical symmetries (Namba and Stubbs, 1985, 1986; Namba et al., 1989). However, the success of fiber diffraction analysis is restricted by how well the layer-line reflections are separated from one another, which depends on how well the fibrous particles are oriented in the filament sol (Holmes, 1995; Makowski, 1991).

F-actin forms mainly two ordered phases of aligned filaments in solution. One is paracrystalline bundles, which are formed by adding polycations (Tang and Janmey, 1996) or polymers such as polyethylene glycol (Suzuki et al., 1989) or in solutions at pH below 5.2 (Kawamura and Maruyama, 1970b). Another is liquid crystalline phases, which are formed at high filament concentrations (Suzuki et al., 1991; Coppin and Leavis, 1992; Furukawa et al., 1993). Well-oriented liquid crystalline sols are the most appropriate specimen for x-ray fiber diffraction analysis, because observed diffraction patterns can be treated as the cylindrical average of the diffraction pattern from the individual filaments.

Filamentous particles spontaneously align with one another when concentrated above a threshold concentration. Formation of liquid crystalline phases of F-actin, namely the transition from the isotropic to the anisotropic phase, has been extensively studied (Suzuki et al., 1989; Coppin and Leavis, 1992; Furukawa et al., 1993). The driving force of such phase transition is attributed to the excluded volume effect of rod-shaped particles, as theoretically pointed out by Onsager (1949) and Flory (1956). Based on much knowledge about the liquid crystalline formation, a systematic method of preparing highly well-oriented liquid crystalline sols of macromolecular assemblies has recently been developed (Yamashita et al., 1998). We applied this method to F-actin sols and tried to find key factors that govern the filament orientation in the sols to attain the best possible orientation. We prepared F-actin sols at various salt concentrations, with filaments of various lengths, which were controlled by gelsolin mixed in polymerization solutions. With these samples, we studied the effect of the filament length and its effective diameter, namely the excluded volume, on the filament orientation and found the optimum condition for producing highly oriented liquid crystalline sols of F-actin. Here we present the results, including a diffraction pattern from the best oriented sol, and discuss the implications of the key factors in the orientation.

Received for publication 18 May 1998 and in final form 24 August 1998.
Address reprint requests to Dr. Toshiro Oda, International Institute for Advanced Research, Matsushita Electric Industrial Co., 3-4 Hikaridai, Seika, Kyoto 619-0237, Japan. Tel.: +0081-774-98-2543; Fax: +0081-774-98-2575; E-mail: toda@crl.mei.co.jp

0006-3495/98/12/2672/10 $2.00

MATERIALS AND METHODS

Preparation of actin and gelsolin

Actin was extracted and purified from the acetone powder of the back and leg muscles of rabbit (New Zealand White) according to the method of Spudich and Watt (1971), with a slight modification (Suzuki and Mihashi,

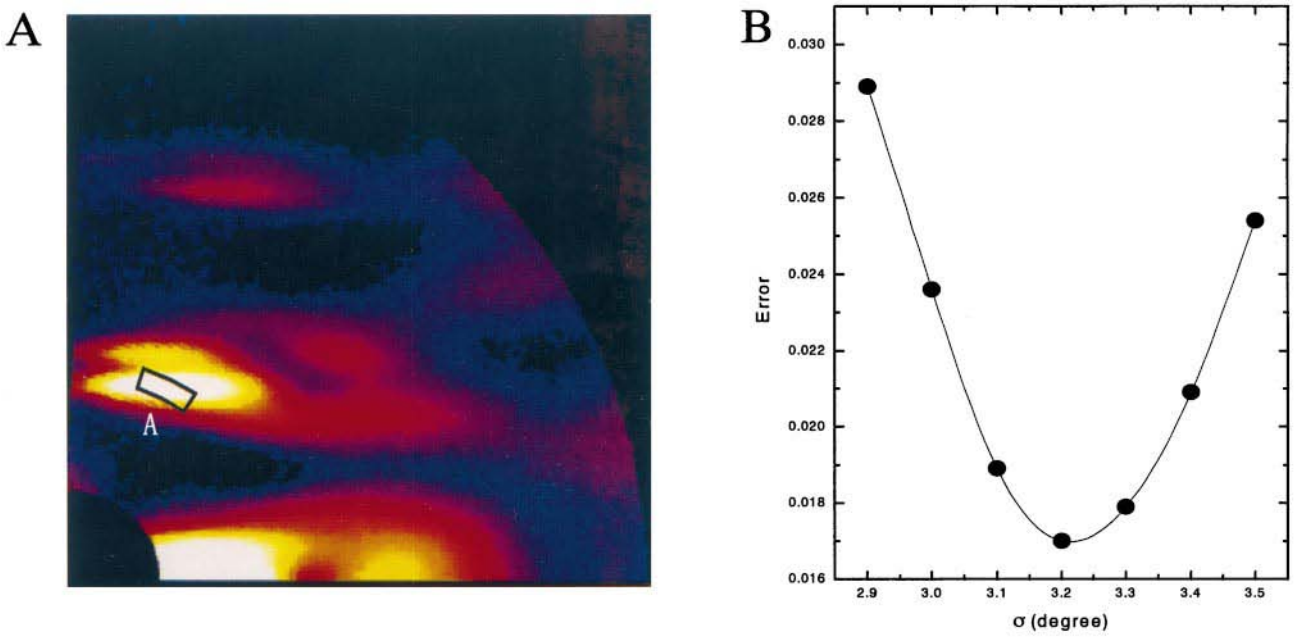

FIGURE 1 (*A*) The curved box is the region (radius = 0.0184–0.0196 $Å^{-1}$, angle = 55–70°) used in determining the standard deviations of filament orientation (σ). The resolution limit of the processed diffraction pattern is 0.05 $Å^{-1}$. (*B*) Typical error behavior for fixed parameter of the standard deviations of filament orientation (σ). The parameter σ was changed manuallly. The data points were interpolated using a spline curve, and the parameter for the minimum error was determined.

1991). Further purification was undertaken by Sephadex G-150 gel filtration (MacLean-Fletcher and Pollard, 1980). Gelsolin was purified from bovine serum according to the method of Kurokawa et al. (1990) and stored at −80° until used.

Preparation of oriented F-actin sols

Gelsolin was added to G-actin solution containing 1 mM $NaHCO_3$, 0.1 mM $CaCl_2$, 0.1 mM ATP, and 1 mM 2-mercaptoethanol, at various molar ratios of actin to gelsolin, to produce desired numbers of nuclei and to control the length distribution of F-actin. After incubation for ~30 min on ice, KCl was added to a final concentration of 60 mM for polymerization of G-actin. The polymerization was undertaken at an actin concentration of 2.0 mg/ml and room temperature. The gelsolin-capped Ca^{2+}-F-actin was used in all experiments. The solution was dialyzed for 2 days, typically against a solution containing 10 mM Tris-HCl (pH 8.0), 30 mM NaCl, 1 mM $CaCl_2$, 0.5 mM ATP, and 1 mM 2-mercaptoethanol. The F-actin solution was centrifuged at 10,000 × *g* for 20 min to remove large aggregations of the filaments. The obtained F-actin filaments were spun down in a low-speed centrifuge at 11,000 × *g* for ~60 h. The resulting soft pellet, namely F-actin sols, was drawn into a quartz capillary with a diameter of 0.7 mm (Müller, Berlin). Some of the samples in the capillary were further centrifuged at 600-2500 × *g* for several days at 4°C. The supernatants were removed after the centrifugation. Finally, a magnetic field of 13.5 Tesla (superconductive magnet; Japan Magnetic Technology, Kobe, Japan) was applied to the F-actin sols at room temperature. The prepared sols were observed and photographed using a microscope equipped with a pair of crossed polarizers.

Recording and processing of x-ray diffraction patterns

X-ray fiber diffraction patterns were recorded on 20 cm × 25 cm Fuji imaging plates, using a Rigaku rotating anode x-ray generator (type RU200) operated at 40 kV and 25 mA and equipped with Ni-coated double-mirror optics. The beam size on the imaging plate was ~0.16 mm (horizontal) × 0.24 mm (vertical). The specimen-to-film distances were ~170 mm, which were calibrated using the diffractions from $CaSO_4 \cdot 2H_2O$ powder crystals. The exposure time was 10 h. The exposed imaging plates were scanned with a Fuji BAS100 system using 0.1-mm rasters. The image data were transferred to a VAX4500 computer and displayed on a D-SCAN GR4416 graphics terminal. The diffraction images in the Cartesian coordinates of the flat film space were converted into the central section of the reciprocal space, and circular symmetric backgrounds were subtracted. Details of the x-ray diffraction pattern recording system were described by Yamashita et al. (1995, 1998).

The upper right patterns of Figs. 3 and 7 were recorded using a Rigaku rotating anode x-ray generator (type FR) operated at 50 kV and 60 mA and equipped with double-mirror optics and an imaging plate x-ray detector system (Rigaku Raxis IV). The beam size on the imaging plate was 0.25 mm (horizontal) × 0.1 mm (vertical). The specimen-to-film distances were ~400 mm. The exposure time was 13 h. The image data were transferred to and processed on a DEC workstation α AX.

Analysis of the diffraction pattern

The angular distributions of the filament orientation in F-actin sols were determined by a two-dimensional profile fitting procedure, as partially described by Yamashita et al. (1995, 1998). Further details will be described elsewhere (Hasegawa et al., manuscript in preparation). Diffraction intensities from perfectly oriented sols of filaments with helical symmetries are limited on layer lines that are separated from one another by the reciprocal of the repeat distance. In reality, the filaments are not exactly parallel to one another, and each spot on the layer lines is smeared into an arc with a finite angular distribution. The direct x-ray beam profile also contributes to the layer-line width. A point-spread function for reconstructing the intensity profile on the central section of the reciprocal space can be calculated by convoluting an angular spread function with the direct beam profile. The angular spread function can be calculated from the angular distribution of the filaments by using the equations deduced by

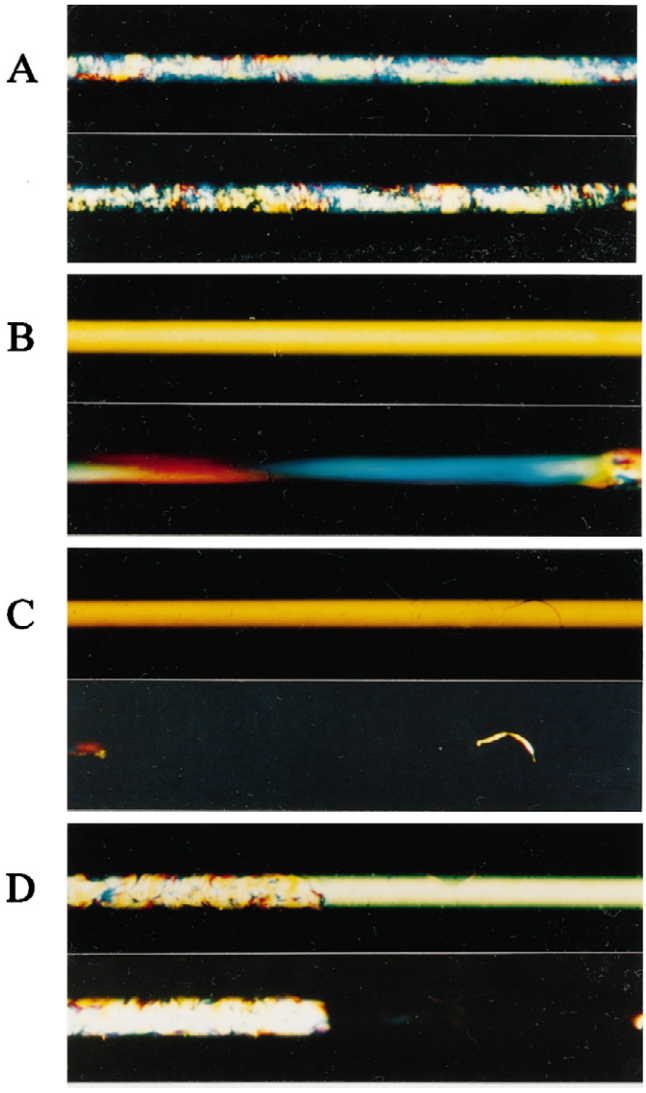

FIGURE 2 Photographs of F-actin sols in the capillary through a polarizing microscope with crossed polarizing plates with the analyzer either at 45° (*upper panels*) or at 90° (*lower panels*) relative to the capillary. (*A*) A sample in the absence of gelsolin. (*B*) A sample in the presence of gelsolin at a molar ratio of 100:1. (*C*) The same sample after a application of a magnetic field of 13.5 Tesla. (*D*) A sample after a low-speed centrifugation and an application of magnetic field of 13.5 Tesla.

Holmes and Barrington-Leigh (1974). The angular distribution of the filaments, $f(\theta)$, can be approximated by a Gaussian (Holmes and Barrington-Leigh, 1974; Makowski, 1978; Yamashita et al., 1998), $f(\theta) \propto \exp(-\theta^2/2\sigma^2)$, where σ is the standard deviation of the distribution. By summing up the point-spread functions weighted by intensities, the intensity profile can be reconstructed, and residuals between the observed and reconstructed profiles obtained pixel by pixel can be minimized in an iterative way to achieve the overall fitting. Local residuals on some layer-line peaks are monitored to find the best fitting values for the variable parameters, such as the width of Gaussians, the repeat distance, and helical symmetry.

The resolution range used for the profile fitting was 0.05–0.08 $Å^{-1}$. A local residual was monitored on the first peak of the 59-Å layer line (*curved box area A* in Fig. 1). When the lattice sampling was observed on this layer line, the near-meridional peak region on the 51-Å layer line was used alternatively, although only rarely. The best fitting parameters were determined on the basis of the local residual by varying the parameters one by one: first, the layer-line position of the 59-Å layer line; then the repeat distance and the helical symmetry; finally, the standard deviation (σ) of the angular distribution of the filaments, as shown in Fig. 1 *B*.

In the model of the ideal liquid of hard spheres, the position of the interference peak is independent of the concentration. However, in the case of F-actin sol, Spencer (1969) showed that the Bragg spacing of interference peak on the equator changes as the actin concentration changes and that the concentration can be calculated from the spacing. Hence the interfilament distance ($d_{f\text{-}f}$) was calculated from the spacing (d) of the first interference peak on the equator as $1.114 \times d$, which is deduced for the interference from the two-dimensional gas model.

Measurement of the filament length

A portion of the sol used for the measurement of the filament orientation was diluted 10,000-fold and was applied to the electron microscopy grids. Negatively stained actin filaments were observed with a JEOL JEM1010 electron microscope at a magnification of 7500×. Electron micrographs were printed, and a circular area with a constant radius was set in the prints. For every filament with its centroid within the circular area, multiple points along the filaments were picked and digitized on the tablet of a D-SCAN GR4416 graphic terminal to calculate the length of the curved filaments, and the data were transferred to VAX workstations. The filament lengths were calculated and the length histograms were constructed.

RESULTS

Formation of homogeneous liquid crystalline

The F-actin filaments were spun down by centrifugation at $11{,}000 \times g$ for ~60 h. The obtained soft F-actin sols were drawn into quartz capillaries with diameters of ~0.7 mm. The F-actin sols were observed and photographed through a polarization microscope with a pair of crossed polarization plates (Fig. 2).

Sols of the F-actin filaments polymerized without gelsolin, which are relatively long, showed mosaic color patterns (Fig. 2 *A*). These small domains did not fuse into a large domain. This may be attributed to the high viscosity of the sols, caused by close packing of the long filaments to a protein concentration as high as 100 mg/ml. As also demonstrated by a report that F-actin solutions formed single uniform domains at concentrations as low as 6 mg/ml, formation of a homogeneous liquid crystalline phase is a diffusion-limited process (Suzuki et al., 1991).

When G-actin was polymerized into F-actin in the presence of gelsolin at an actin/gelsolin molar ratio of 100:1, the average length of F-actin was ~350 nm (Table 1). The F-actin sols with this short average filament length formed a large homogeneous domain spontaneously only several hours after being drawn into the capillary. The large domain was bright when the capillary axis was at 45° to the analyzer (Fig. 2 *B, upper panel*) and dark at 90° (Fig. 2 *B, lower panel*). This remarkably high birefringence, which is a characteristic of a liquid crystalline phase, indicates that the filaments are aligned along the capillary axis. After these sols were left in a magnetic field of 13.5 Tesla for 1 day with the capillary axis parallel to the field, the slight color undulation observed at the 90° position before the magnetic treatment (Fig. 2 *B, lower panel*) disappeared completely

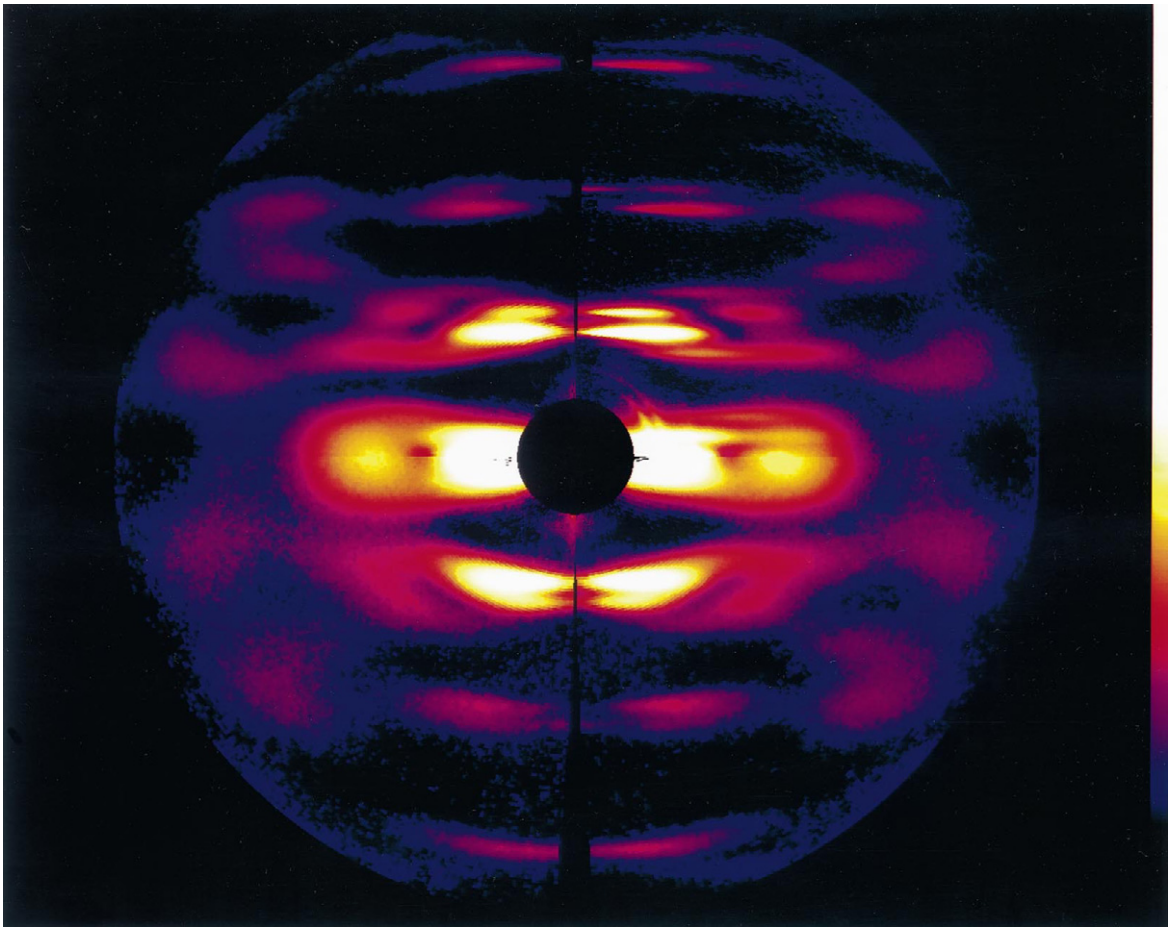

FIGURE 3 The correspondence between standard deviations of filament orientation and the diffraction pattern: $\sigma = 5.3$ (*lower left*); $\sigma = 4.1$ (*lower right*); $\sigma = 3.0$ (*upper left*). The edge of these patterns corresponds to the 16-Å resolution. The upper right quarter is a best pattern of F-actin ($\sigma < 2$), which was obtained by removal of salt with an ion-exchange gel.

(Fig. 2 *C, lower panel*). The filaments in the sols were therefore oriented parallel to the magnetic field (Torbet and Dickens, 1984).

Effect of the salt concentration and pH on the filament orientation

Electrostatic interactions between charged rod-like particles strongly influence the formation of the liquid crystalline phase. For instance, it has been reported that the minimum concentration of tobacco mosaic virus (TMV) necessary for the transition from an isotropic to anisotropic phase decreases with the ionic strength of the solvent (Oster, 1950). We studied the effect of pH (6.0–8.5) and the ionic strength (30, 60, and 90 mM NaCl) of the solvent on the filament orientation in the sols. Relatively short F-actin filaments (average length 350 nm), polymerized in the presence of gelsolin at the molar ratio of 100:1, were used for this experiment. X-ray diffraction patterns were recorded after applying the 13.5-Tesla magnetic field for 1–3 days. All of the samples formed a homogeneous domain, except for those prepared in solvents containing 90 mM NaCl at pH 6 and 6.5.

Interfilament distances and standard deviations of the angular distributions of the filament orientations were extracted from x-ray diffraction patterns. As was done by Spencer (1969), the filament concentrations were estimated from the interfilament distances. To compare the angular distributions of the filament orientations at various filament concentrations, the standard deviations of the distributions (σ) were plotted as a function of the squared interfilament distance ($d^2_{\text{f-f}}$), which is inversely proportional to the filament density in the plane of the cross section of the sols. Representative diffraction patterns for four different standard deviations of the distributions (σ) are shown in Fig. 3.

In Fig. 4 *A*, data points are labeled for the salt concentrations. The data points were segregated into three regions according to the ionic strength. Regardless of the ionic strength, the standard deviations are smaller when the interfilament distances are small. This result indicates that the filaments are better oriented when packed closer.

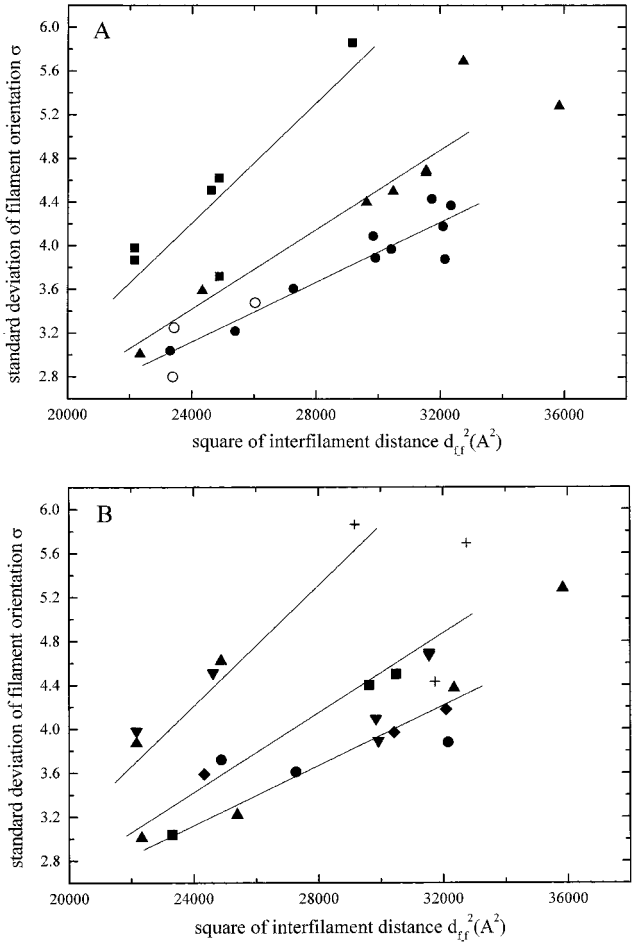

FIGURE 4 The relationship between the standard deviation of filament orientation (σ) and the square of the interfilament distance. In graph A the data points are labeled according to the NaCl concentration of the solvent; 30 mM (●), 60 mM (▲), 90 mM (■). The filled circles are from the sols without additional centrifugation in the capillary. The open circles are from the sols at 30 mM NaCl with additional centrifugation at low speed. The lines are linear regressions for data points (●), and the slopes are 1.37×10^{-4}, 1.82×10^{-4}, and 2.74×10^{-4} Å^{-2} at 30 mM, 60 mM and 90 mM, respectively. In graph B, the same sets of data points as for graph A are now labeled according to the pH of the solvent: 8.5 (+); 8.0 (▲); 7.5 (▼); 7.0 (●); 6.5 (♦); 6.0 (■). The lines are identical to those in graph A. The solvent condition was 10 mM Tris-acerate (pH 8.5, 8.0, 7.5)/10 mM bis-Tris-acetate (pH 7.0, 6.5, 6.0), 1 mM $CaCl_2$, 0.5 mM ATP, and 1 mM 2-mercaptoethanol, with various concentrations of NaCl. F-actin with gelsolin at a ratio of 100:1 was used.

At any interfilament distance, the smallest standard deviation was obtained at 30 mM NaCl, and it was greatest at 90 mM NaCl. This means that the filaments are better oriented at relatively low ionic strength. The lines in Fig. 4 were obtained by linear regression of the data for each NaCl concentration. The slope of the line is steeper in order of 30 and 60 mM and the steepest at 90 mM NaCl. The orientation of the filaments thus shows a larger dependence on their packing at higher ionic strength.

The surface charge density of actin increases with pH, according to the pH titration data (Martonosi et al., 1964). However, the filament orientation did not show any systematic dependence on the solvent pH (Fig. 4 *B*).

Concentration by low-speed centrifugations

F-actin sols prepared at 30 mM NaCl and drawn into capillaries were concentrated by low-speed centrifugation in two steps, $1400 \times g$ for 3 days and $2500 \times g$ for 3 days. The centrifugation disturbed the homogeneous sols, but single homogeneous domains were reformed by application of the strong magnetic field, except the bottom half of the sols (Fig. 2 *D*). The standard deviations of the filament orientations (*open circles* in Fig. 4 *A*) were relatively small and along the linear regression line for the data obtained from the sols before this centrifugation. For example, the standard deviation decreased from 3.6° to 2.8° when the interfilament distance decreased from 16 nm to 15 nm by a long centrifugation. This result showed that this slow and long centrifugation is effective in reducing the interfilament distance and improving the filament orientation.

By even slower and longer centrifugation, for example, sequential centrifugation of $600 \times g$ for 3 days, $1400 \times g$ for 3 days, and $2500 \times g$ for 8 days, followed by magnetic orientation with a 13.5-Tesla field, x-ray diffraction patterns from some of these sols showed many lattice sampling reflections on layer lines as well as on the equator. In typical cases, the 51-Å, 59-Å, and 356-Å layer lines showed such sampling, which were not necessarily mirror-symmetrical with the meridian. However, no sampling was observed on the 27-Å layer line, unlike in the case of partially dried F-actin sols (Lednev and Popp, 1990). The interfilament distances in these sols were ~15 nm, which is much larger than the diameter of the F-actin filament. This indicates that the filaments form partial three-dimensional lattices when the filaments are closely packed to a lateral distance of ~15 nm at 30 mM NaCl.

Effect of the filament length on the filament orientation

A critical concentration necessary for the transition to liquid crystalline phases is strongly dependent on the average length of F-actin; the shorter the filaments, the higher the filament concentration required for the transition (Suzuki et al., 1991). We examined the effect of average filament length on the filament orientation. Gelsolin was used to control the filament length (Janmey et al., 1986). First, the filament length distribution in each sol was measured by electron microscopy. The distribution was an exponential type function as in Fig. 5, as pointed out theoretically by Oosawa (Oosawa and Asakura, 1975) and shown by previous experiments (Kawamura and Maruyama, 1970a; Janmey et al., 1986). The average lengths are listed in Table 1 for the filaments prepared at various molar ratios of actin to gelsolin. Even the smallest aspect ratio (length/diameter) of these filaments, which is 220/15 = 15 for an effective

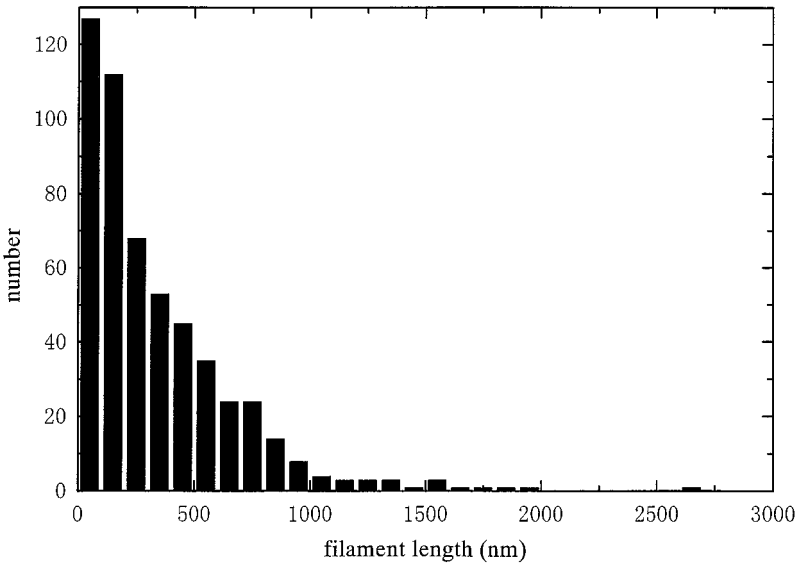

FIGURE 5 Length distribution of F-actin in the sols collected by centrifugation. The graph is a typical histogram obtained from F-actin prepared in the presence of gelsolin at a molar ratio of 100:1. The average length was 350 Å (n = 532). The ratio of the weight-averaged length to the number-averaged length was 1.9, which is close to the theoretical value by Oosawa (Oosawa and Asakura, 1975). The solvent condition was 10 mM Tris-acetate (pH 8.0), 30 mM NaCl, 1 mM $CaCl_2$, 0.5 mM ATP, and 1 mM 2-mercaptoethanol.

filament diameter of 15 nm, is large enough for the filaments to behave as rod-shaped particles. The average lengths of the filament prepared at lower molar ratios were much longer than those predicted from the molar ratio; for instance, the length at a ratio of 40 would be predicted to be 2.7 nm (filament length per subunit) times 40, ~110 nm, but the observation was 220 nm. This discrepancy may be caused by the centrifugation at 11,000 × g to make F-actin sols, by which only relatively long filaments were collected. The amount of collected F-actin in sols was actually only half of the total protein in the solution before the centrifugation. The discrepancy at the higher ratios of 400 and 800 could be due to the filament breakage during sample preparation for electron microscopy (Janmey et al., 1986) and/or to spontaneous nucleation without gelsolin because of the relatively high actin concentration (2 mg/ml) used for polymerization.

The standard deviations of the filament orientation (σ) are plotted as a function of the squared interfilament distance in Fig. 6. By comparing the data for the ratio of 40 with those for 400, it is clear that F-actin sols of the filaments with a longer average length are better oriented, regardless of the interfilament distance. However, the standard deviations of the filament orientations of the sols show similar values between those prepared at the ratios of 400 and 800, i.e., at average lengths of 630 nm and 1130 nm, respectively. These results suggest that the filament orientation improves with increase in filament length and reaches a limit around an average length of 600 nm. On the other hand, the slopes of σ versus $d^2_{f\text{-}f}$ did not show any significant difference, as indicated by the two linear regression lines for the data obtained at the ratios of 40 and 400, i.e., at average lengths of 220 nm and 630 nm, respectively. This means that the average filament length does not have much effect on the concentration dependence of the filament orientation, in contrast to that of the effective diameter, which can be modified by the NaCl concentration in the solvents, as shown in Fig. 4 *A*.

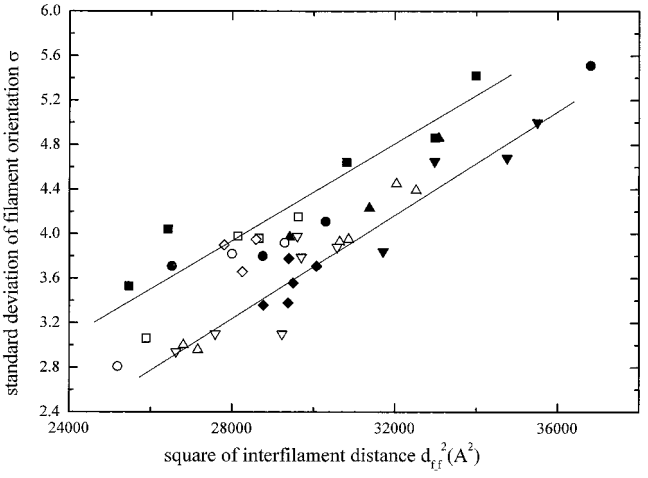

FIGURE 6 The relationship between the square of the interfilament distances and the standard deviations of filament orientation (σ), which are classified according to the ratio of actin to gelsolin: 40:1 (■), 100:1 (●), 200:1 (▲), 400:1 (▼), and 800:1 (♦). ●, Capillaries without additional centrifugation in the capillary; ○, capillaries with additional centrifugation. The solvent condition was the same as in Fig. 4 with 30 mM NaCl. The linear regression coefficients are 2.17×10^4 Å^{-2} for 40:1 and 2.32×10^{-4} Å^{-2} for 400:1.

TABLE 1 Molar ratio of actin to gelsolin and average lengths of the polymerized filaments

Molar ratio	40	100	200	400	800
Number*	550	532	321	232	162
Average length (nm)	220	350	570	630	1130
Predicted length (nm)	110	270	540	1080	2160

*Number of F-actin filaments used for the measurement of length.

DISCUSSION

The experimental procedures developed to prepare well-oriented F-actin sol as described in Materilas and Methods and the Results of the present study were designed based on the multiple steps method for aligning filamentous assemblies of macromolecules described by Yamashita et al. (1998). The multiple steps involve liquid crystallization, slow centrifugation, and magnetic orientation. The optimal condition for liquid crystallization should in principle be much less dependent on the component proteins than that for crystallization, because the former is a kind of physical process, whereas the latter deeply involves chemical processes. The optimal solution conditions for protein crystallization show a wide variety from protein to protein because formation of crystal arrays relies on direct contacts between amino acid residues of the protein surface and therefore is heavily affected by the amino acid sequences and surface structures of proteins. In liquid crystalline phases, the filamentous assemblies do not touch one another directly. A balance between packing forces against concentration of the filamentous particles and weak electrostatic repulsive forces between those polyelectrolytes is the major driving force that promotes mutual alignment of the particles. Therefore, any method of liquid crystallization that works well on a particular system should be more or less applicable to various types of protein assemblies. In the present study, we demonstrated that the method proposed by Yamashita et al. (1998), which worked well on bacterial flagellar filaments and TMV, is effective for orienting F-actin sols as well. However, our results also revealed some specific modifications essential for orienting F-actin sols.

We first describe the basic parameters that determine the orientation of filamentous particles in the nematic liquid crystalline phase and then try to interpret the results and discuss their implications by comparing the data with those predicted by these basic parameters.

The basic parameters that determine orientation

Onsager (1949) developed a theoretical treatment that deals with the important parameters in the formation of the nematic phase by rod-shaped particles of length L and diameter D in solution, based on a description of the free energy by the second virial approximation. In minimizing the free energy of such a system, the orientational entropy (or confinement) and the second virial coefficient, which in this case is the product of the mutual excluded volume averaged over a given angular distribution between two rods and the number concentration of rods, play crucial roles; a balance between these two parameters determines the angular distribution function, namely the orientational distribution of the rods. According to Odijk (1986), who assumed a Gaussian distribution with a standard deviation of σ, the free energy is determined by sum of the orientational entropy ($\sim 1 - \ln(1/\sigma^2)$) and the mutual excluded volume ($\sim \pi^{1/2} L^2 D\sigma$) times the number concentration (N/V, where N is the number of rods and V is the total volume). Free energy minimization results in σ being inversely proportional to L^2DN/V. The diameter of the rod, D, can be replaced by D_{eff}, which is the effective diameter of the rod, which is determined by the electrostatic interactions between the rods in solution. The number concentration is approximately proportional to $d_{\text{f-f}}^{-2} L^{-1}$, where $d_{\text{f-f}}$ is the average lateral distance between the rods. Thus the standard deviation σ is proportional to $(D_{\text{eff}}L)^{-1} d_{\text{f-f}}^2$. This relationship means that the longer the rod, the larger its effective diameter, and the higher its concentration, the better the rods are oriented.

Salt concentration dependence

The data presented in the Results showed that the best orientation of F-actin sols was obtained at 30 mM NaCl, the lowest ionic strength among those examined. In solutions of low ionic strength, the electrostatic repulsive force between the F-actin filaments is relatively large, which makes the effective diameter D_{eff} of the filament relatively large. Based on the theoretical treatment of the system described in the previous section, we can predict that the standard deviation σ of the angular distribution function is smaller at lower ionic strength because of the larger effective diameter. The data in Fig. 4 *A* clearly show that at any given interfilament distance, the smallest standard deviation is obtained at 30 mM and the largest one at 90 mM.

The slopes of the lines in Fig. 4 *A*, namely $\Delta\sigma/\Delta d_{\text{f-f}}^2$, is also supposed to be proportional to $(D_{\text{eff}}L)^{-1}$ by the theoretical treatment. Because the data in Fig. 4 *A* were obtained from the F-actin filaments with the same length distribution, the slopes should be inversely proportional to D_{eff}; in other words, the slope should be larger for the data obtained at higher ionic strength. The data in Fig. 4 *A* are roughly consistent with this prediction.

Length dependence

As shown in Fig. 6, the better orientation was obtained when the average length of the F-actin filaments was longer, at least up to an average length of 600 nm. This relation is more or less consistent with the prediction, although only qualitatively, that the standard deviation becomes smaller as the filament length L increases at any given interfilament distance.

The theoretical treatment also suggests that the slope of the line, $\Delta\sigma/\Delta d_{\text{f-f}}^2$, is inversely proportional to the length L. However, the slopes of the two lines, one for the data with an average length of 220 nm and the other for those with an average length of 630 nm, are roughly the same and do not really show L^{-1} dependence. We do not have a good explanation for this discrepancy.

Limitation of the orientation of flexible filaments

Even the relation of the orientation versus the average filament length does not hold beyond an average length

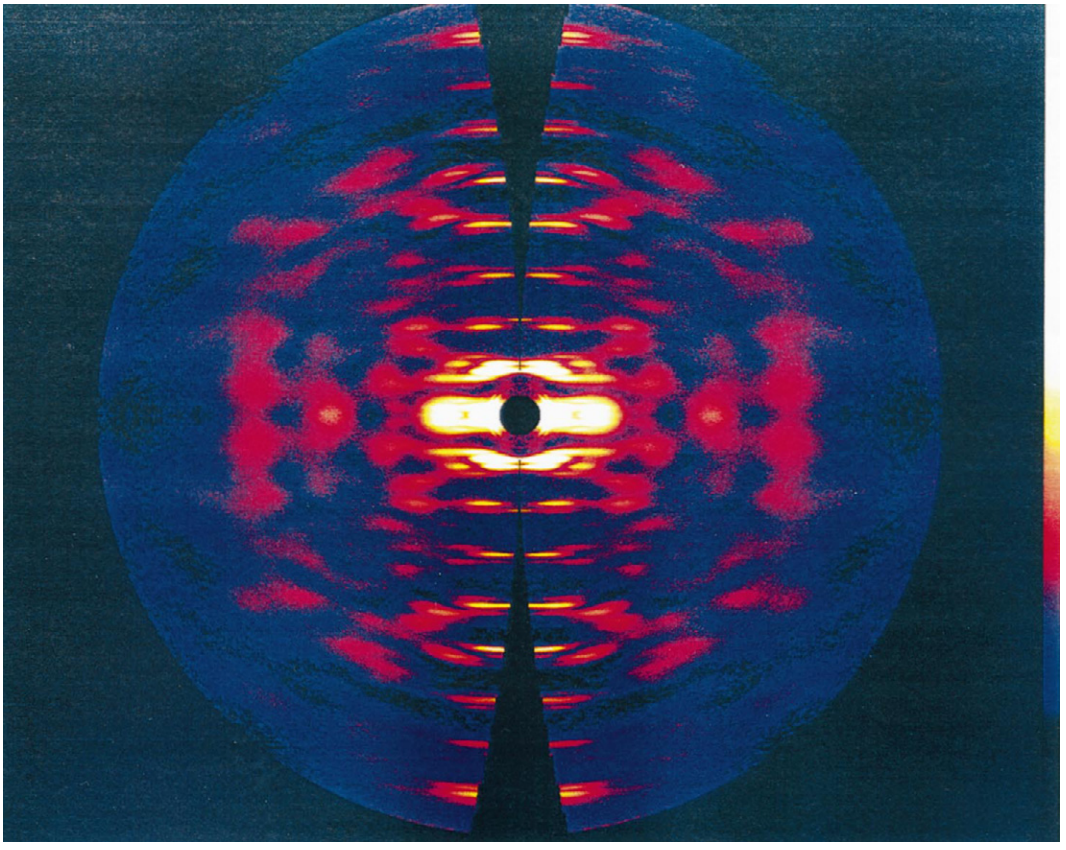

FIGURE 7 The best diffraction pattern of F-actin sol. The pattern is the same as the upper light quarter pattern in Fig. 3. The resolution limit is 6 Å.

longer than 600 nm, and there seems to be a lowest limitation of the standard deviation that can be obtained by increasing the filament length, at a given interfilament distance and effective diameter. The reason for this appears to come from the fact that, although the theoretical prediction assumes the filament is a hard rod, the F-actin filament is relatively flexible. This can be more or less intuitively understood by thinking of the orientational confinement of a rod within a virtual tubular wall formed by a set of rods that surrounds the central rod with roughly parallel alignments (Odijk, 1985). If the thermal motion of a filament within a tubular wall is considered as in the previous section, a short filament would make contacts with the wall only at its ends, because the bending curvature by its flexibility would be negligibly small, but a long filament would make multiple contacts, because the bending would be significantly large. Therefore, the standard deviation of filament orientation observed by x-ray fiber diffraction becomes smaller as the filament length increases, but only up to some point determined by the flexibility of the filament. Beyond that point, the orientation cannot be further improved.

The boundary point of the filament length can be roughly predicted from known mechanical parameters of the F-actin filament. We can consider a situation in which a bent filament makes contacts with the tubular wall at three points, both ends and the middle; that is, the amplitude of the bend is the same as the effective diameter of the tubular wall, which is $2(d_{\text{f-f}} - D_{\text{eff}})$. If we use experimentally obtained values, 18 nm for $d_{\text{f-f}}$ and 15 nm for D_{eff}, the effective diameter of the tube is 6 nm. The first-order thermal bending of the F-actin filament, which gives the largest bending amplitude, can be calculated as done by Fujime (1970), using its persistence length of $\sim$10 μm (Isambert et al., 1995), to be $\sim$6 nm when the filament length is 400 nm. This estimate is roughly in the same range as the experimentally obtained limiting length, 600 nm, indicating the validity of this explanation. The consideration also suggests that there is an effective filament length for the orientation. Thus a further improvement of the orientation is expected either by decreasing $d_{\text{f-f}}$ by further concentration or by somehow making the filament much stiffer.

The F-actin filaments polymerized by adding KCl to the monomer solution in the presence of Ca^{2+} and ATP were observed to be significantly stiffer than those prepared in other conditions, probably because of the bound nucleotide and divalent cation (Orlova and Egelman, 1993). The F-actin filaments we used throughout the present study were prepared under these conditions, and this may have contributed to the significantly better orientation of the sols we obtained compared to those in literature.

Weak pH dependence

As shown in Fig. 4 *B*, the filament orientation did not show any systematic dependence on the solvent pH, in contrast to the ionic strength, despite the fact that the negative charge density of the F-actin filament is supposed to increase as the solvent pH increases from 6 to 8, because the isoelectric pH is ~5.4 (Garrels and Gibson, 1976). This suggests that the net charge density affects the electrostatic interactions between the filaments much less than the shielding effect by counterions. In general, the apparent charge density of macromolecules with many charges (the charge density recognized from a short distance) is insensitive to the net charge density because of the nonlinear electrostatic screening effect (Oosawa, 1971). The nonlinear screening effect occurs regardless of the form of the macromolecule but is most remarkable in the case of a thin and long charged rod such as DNA, the diameter of which is ~2 nm (Manning, 1978). A theoretical study has also shown that the effective diameter of a highly charged rod is only weakly dependent on the net charge, even for rods thicker than DNA, such as TMV, the diameter of which is 18 nm (Stroobants et al., 1986). Because the F-actin filament has a highly charged surface around the N-terminus of each subunit, it would be the cause of the weak pH dependence of the effective diameter of this filament, which determines the standard deviation of the orientation.

The effective diameter of F-actin

Lattice sampling was observed even on layer lines as well as on the equator when F-actin sols were highly concentrated by long slow centrifugation at 30 mM NaCl. The interfilament distances obtained from the peak positions on the equator were ~15 nm, which is still much larger than the actual diameter of the filament, 9–9.5 nm, as obtained from an atomic model by Holmes et al. (1990), or 10 nm, in the refined model of Lorenz et al. (1993). This suggests that a long-range repulsion between the F-actin filaments is present, and the repulsion is modulated periodically along the filament so that it interlocks the filaments in an axial register as well as in the lateral one. The interlocking may limit the free sliding motion along the axis of the alignment observed in the liquid crystalline phase (Käs et al., 1996). According to the atomic model of F-actin (Holmes et al., 1990), the negative charges are highly localized around the N-terminus of the subunit. Correspondingly, a large negative electrostatic potential is distributed along the helical form of the filament (Nakamura et al., 1994). It is likely that this periodic distribution of the electrostatic potential along the filament is responsible for the interlocked filaments in the concentrated sols.

Thus the effective diameter, D_{eff}, of the F-actin filament at 30 mM NaCl is estimated to be 15 nm. A similar size was obtained from the recognition distance between the myosin head and the F-actin filament measured by atomic force microscopy in a low-ionic-strength solvent (Nakajima et al., 1997); the interaction is believed to be electrostatic. This effective diameter of 15 nm at 30 mM NaCl and the theoretical prediction in the previous section that the slope $\Delta\sigma/\Delta d_{\mathrm{f\text{-}f}}^2$ is proportional to $(D_{\mathrm{eff}}L)^{-1}$ allow us to estimate the effective diameters at higher salt concentrations. From the slopes of the lines in Fig. 4 *A*, the effective diameter is estimated to be 12 nm at 60 mM and 8 nm at 90 mM NaCl. The effective diameter of 8 nm is even smaller than the diameter of the atomic model, but this would be plausible if interlocking of the two-stranded long-pitch helical ribbon structure is considered. These values are more or less comparable to the one obtained by Matsudaira et al. (1983), which is ~12 nm at 75 mM NaCl. In any case, the filaments were better oriented at any interfilament distances when the effective diameter is larger, as shown in Fig. 4 *A*.

CONCLUSION

We found a strategy that works well for preparing highly well-oriented F-actin sols: use a very slow (600–2500 × *g*) and long (several days) centrifugation to concentrate the F-actin filaments, the average length of which is controlled at ~0.6 μm by using gelsolin for polymerization of the filament, in a solution with an ionic strength that is low as possible, typically less than 30 mM NaCl, and expose the sols to a strong magnetic field (Fig. 7).

We thank Mr. K. Hasegawa for technical help in x-ray fiber diffraction data collection and data processing. We also thank Drs. F. Oosawa and K. Mihashi for their encouragement.

REFERENCES

Coppin, C. M., and P. C. Leavis. 1992. Quantitation of liquid-crystalline ordering in F-actin solutions. *Biophys. J.* 63:794–807.

Flory, P. J. 1956. Phase equilibria in solutions of rod-like particles. *Proc. R. Soc. Lond. A.* 234:73–89.

Fujime, S. 1970. Quasi-elastic light scattering from solutions of macromolecules. II. Doppler broadening of light scattered from solutions of semi-flexible polymers, F-actin. *J. Phys. Soc. Jpn.* 29:751–759.

Furukawa, R., R. Kundra, and M. Fechheimer. 1993. Formation of liquid crystals from actin filaments. *Biochemistry.* 32:12346–12352.

Garrels, J. I., and W. Gibson. 1976. Identification and characterization of multiple forms of actin. *Cell.* 9:793–805.

Hanson, J., and S. Lowy. 1963. The structure of F-actin and of actin filaments isolated from muscle. *J. Mol. Biol.* 6:46–60.

Holmes, K. C. 1995. Solving the structure of macromolecular complexes with the help of x-ray fiber diffraction diagrams. *J. Struct. Biol.* 115: 151–158.

Holmes, K. C., and J. Barrington-Leigh. 1974. The effect of disorientation on the intensity distribution of non-crystalline fibers. I. Theory. *Acta Crystallogr. A.* 30:635–638.

Holmes, K. C., D. Popp, W. Gebhard, and W. Kabsch. 1990. Atomic model of the actin filament. *Nature.* 347:44–49.

Isambert, H., P. Venier, A. C. Maggs, A. Fattoum, R. Kassab, D. Pantaloni, and M.-F. Carlier. 1995. Flexibility of actin filaments derived from thermal fluctuations. Effect of bound nucleotide, phalloidin, and muscle regulatory proteins. *J. Biol. Chem.* 270:11437–11444.

Janmey, P. A., J. Peetermans, K. S. Zaner, T. P. Stossel, and T. Tanaka. 1986. Structure and mobility of actin filaments as measured by quasielastic light scattering, viscometry, and electron microscopy. *J. Biol. Chem.* 261:8357–8362.

Kabsch, W., H. G. Mannherz, D. Suck, E. F. Pai, and K. C. Holmes. 1990. Atomic structure of the actin:DNase I complex. *Nature.* 347:37–44.

Käs, J., H. Strey, J. X. Tang, D. Finger, R. Ezzell, E. Sackmann, and P. A. Janmey. 1996. F-actin, a model polymer for semiflexible chains in dilute, semidilute, and liquid crystalline solutions. *Biophys. J.* 70: 609–625.

Kawamura, M., and K. Maruyama. 1970a. Electron microscopic particle length of F-actin polymerized in vitro. *J. Biochem. (Tokyo).* 67: 437–457.

Kawamura, M., and K. Maruyama. 1970b. Polymorphism of F-actin. I. Three forms of paracrystals. *J. Biochem. (Tokyo).* 68:885–899.

Kurokawa, H., W. Fujii, K. Ohmi, K. T. Sakurai, and Y. Nonomura. 1990. Simple and rapid purification of brevin. *Biochem. Biophys. Res. Commun.* 168:451–457.

Lednev, V. V., and D. Popp. 1990. Supercoiling of F-actin filaments. *J. Struct. Biol.* 103:225–231.

Lorenz, M., D. Popp, and K. Holmes. 1993. Refinement of the F-actin model against x-ray fiber diffraction data by the use of a directed mutation algorithm. *J. Mol. Biol.* 234:826–836.

MacLean-Fletcher, S. D., and T. D. Pollard. 1980. Identification of a factor in conventional muscle actin preparations which inhibits actin filament self-association. *Biochem. Biophys. Res. Commun.* 96:18–27.

Makowski, L. 1978. Processing of X-ray diffraction data from partially oriented specimens. *J. Appl. Crystallogr.* 11:273–283.

Makowski, L. 1991. An estimate of the number of structural parameters measurable from a fiber diffraction pattern. *Acta Crystallogr. A.* 47: 562–567.

Manning, G. S. 1978. The molecular theory of polyelectrolyte solutions with applications to the electrostatic properties of polynucleotides. *Q. Rev. Biophys.* 11:179–246.

Martonosi, A., C. M. Molino, and J. Gergely. 1964. The binding of divalent cations to actin. *J. Biol. Chem.* 239:1057–1064.

Matsudaira, P., E. Mandelkow, W. Renner, L. K. Hesterberg, and K. Weber. 1983. Role of fimbrin and villin in determining the interfilament distances of actin bundles. *Nature.* 301:209–214.

McLaughlin, P. J., J. T. Gooch, H. G. Mannherz, and A. G. Weeds. 1993. Structure of gelsolin segment 1-actin complex and the mechanism of filament severing. *Nature.* 364:685–692.

Milligan, R. A., M. Whittaker, and D. Safer. 1990. Molecular structure of F-actin and location of surface binding sites. *Nature.* 348:217–221.

Nakajima, H., Y. Kunioka, K. Nakano, K. Shimizu, M. Seto, and T. Ando. 1997. Scanning force microscopy of the interaction events between a single molecule of heavy meromyosin and actin. *Biochem. Biophys. Res. Commun.* 234:178–182.

Nakamura, H., S. Nagashima, and T. Wakabayashi. 1994. Electrostatic field around the actin filament. *In* Synchrotron Radiation in the Biosciences. B. Chance, J. Deisenhofer, S. Ebashi, D. T. Goodhead, J. R. Helliwell, H. E. Huxley, T. Iizuka, J. Kirz, T. Mitsui, E. Rubenstein, N. Sakabe, T. Sasaki, G. Schmahl, H. B. Stuhrmann, K. Wüthrich, and G. Zaccai, editors. Clarendon Press, Oxford. 502–508.

Namba, K., R. Pattanayek, and G. Stubbs. 1989. Visualization of protein-nucleic acid interactions in a virus. Refined structure of intact tobacco mosaic virus at 2.9 Å resolution by x-ray fiber diffraction. *J. Mol. Biol.* 208:307–325.

Namba, K., and G. Stubbs. 1985. Solving the phase problem in fiber diffraction. Application to tobacco mosaic virus at 3.6 Å resolution. *Acta Crystallogr. A.* 41:252–262.

Namba, K., and G. Stubbs. 1986. Structure of tobacco mosaic virus at 3.6 Å resolution: implications for assembly. *Science.* 231:1401–1406.

Odijk, T. 1985. Scaling theory of the isotropic-liquid crystalline phase transition in a solution of wormlike polymers. *Polym. Commun.* 26: 197–198.

Odijk, T. 1986. Theory of lyotropic polymer liquid crystals. *Macromolecules.* 19:2313–2329.

Onsager, L. 1949. The effects of shape on the interaction of colloidal particles. *Ann. N.Y. Acad. Sci.* 51:627–659.

Oosawa, F. 1971. Polyelectrolytes. Marcel Dekker, New York. 13–25.

Oosawa, F., and S. Asakura. 1975. Thermodynamics of the Polymerization of Protein. Academic Press, San Diego. 25–40.

Orlova, A., and E. H. Egelman. 1993. A conformational change in the actin subunit can change the flexibility of the actin filament. *J. Mol. Biol.* 232:334–341.

Oster, G. 1950. Two-phase formation in solutions of tobacco mosaic virus and the problem of long-range forces. *J. Gen. Physiol.* 33:445–473.

Popp, D., V. V. Lednev, and W. Jahn. 1987. Methods of preparing well-orientated sols of F-actin containing filaments suitable for x-ray diffraction. *J. Mol. Biol.* 197:679–684.

Schutt, C. E., J. C. Myslik, M. D. Rozycki, N. C. W. Goonesekere, and U. Lindberg. 1993. The structure of crystalline profilin-β-actin. *Nature.* 365:810–816.

Spencer, M. 1969. Low-angle X-ray diffraction from concentrated sols of F-actin. *Nature.* 223:1361–1362.

Spudich, J. A., and S. Watt. 1971. The regulation of rabbit skeletal muscle contraction. I. Biochemical studies of the interaction of the tropomyosin-troponin complex with actin and the proteolytic fragments of myosin. *J. Biol. Chem.* 246:4866–4871.

Stroobants, A., H. N. W. Lekkerkerker, and T. Odijk. 1986. Effect of electrostatic interaction on the liquid crystal phase transition in solutions of rodlike polyelectrolytes. *Macromolecules.* 19:2232–2238.

Suzuki, A., T. Maeda, and T. Ito. 1991. Formation of liquid crystalline phase of actin filament solutions and its dependence on filament length as studied by optical birefringence. *Biophys. J.* 59:25–30.

Suzuki, N., and K. Mihashi. 1991. Binding mode of cytochalasin B to F-actin is altered by lateral binding of regulatory proteins. *J. Biochem. (Tokyo).* 109:19–23.

Suzuki, A., M. Yamazaki, and T. Ito. 1989. Osmoelastic coupling in biological structures: formation of parallel bundles of actin filaments in a crystalline-like structure caused by osmotic stress. *Biochemistry.* 25: 6513–6518.

Tang, J. X., and P. A. Janmey. 1996. The polyelectrolyte nature of F-actin and the mechanism of actin bundle formation. *J. Biol. Chem.* 271: 8556–8563.

Torbet, J., and M. J. Dickens. 1984. Orientation of skeletal muscle actin in strong magnetic fields. *FEBS Lett.* 173:403–406.

Yamashita, I., H. Suzuki, and K. Namba. 1998. Multiple-step method for making exceptionally well oriented liquid-crystalline sols of maromolecular assemblies. *J. Mol. Biol.* 278:609–615.

Yamashita, I., F. Vonderviszt, Y. Mimori, H. Suzuki, K. Oosawa, and K. Namba. 1995. Radial mass analysis of the flagellar filament of *Salmonella*: implications for the subunit folding. *J. Mol. Biol.* 253: 547–558.